Influence of Ceramic Aggregate on Cast Iron Properties

Scott R. Giese
University of Northern Iowa, Cedar Falls, Iowa, USA

Justine Radunzel
University of Northern Iowa, Cedar Falls, Iowa, USA

ABSTRACT

Because of the Occupational Safety And Health Administration (OSHA) Silica Rule under enforcement in the foundry industry today, many iron foundries have or are considering changing from silica sand to a ceramic aggregate to alleviate the issue. The AFS Cast Iron Research Committee initiated a research project to understand the impact of the change in the microstructure and associated mechanical properties on cast iron that might accompany the use of these ceramic molding media. Funded by the American Foundry Society (AFS) and Ductile Iron Society (DIS), a research project was performed to assess the mechanical properties of class 40 gray iron and 80-55-06 ductile iron castings using an experimental casting matrix of the three aggregates with two sand to metal ratios. Results indicated that ceramic aggregates have a noticeable influence on the mechanical properties of gray and ductile iron but the sand to metal ratio has an influence on the degree of property variation.

Keywords: ceramic aggregates, silica sand, ductile iron, gray iron, and mechanical properties

INTRODUCTION

Due to the OSHA Silica Rule under enforcement in the foundry industry today, one scenario that many foundries are considering is a change from silica sand, used in most foundries today, to ceramic sand/media to alleviate the issue. There are many questions associated with this change, but one that is of primary importance is understanding the change, if any, in microstructure and the associated mechanical properties that might accompany the use of ceramic sand/media.

The American Foundry Society funded two research projects in the mid-2010's investigating the use of ceramic molding aggregates, mostly focused on the substitution of this aggregate in clay-bonded green sand molding operations.[1-3] The primary objective of the investigations addressed foundry concerns in casting surface, surface defects (in terms of metal penetration and veining), attrition losses, and sand reclamation. The AFS Cast Iron Research Committee and Ductile Iron Society initiated a research program exploring the influence of ceramic aggregates leading to changes in solidification behaviors affecting the microstructure and mechanical properties of gray and ductile iron castings. Presently, information is not available for the foundry industry to understand how thermal physical characteristics can influence subtle casting design and metallurgical changes leading to potentially costly tooling alterations and mechanical properties specifications.

DESIGN OF EXPERIMENTS

The first component of the project was to design a casting that (a) has features such that tensile test bars could be extracted to provide a representative variation of mechanical properties based on cooling rate using section thickness as the control and (b) the pattern could be easily retooled for investigating the influence of sand to metal ratio. The sand to metal ratio approved by the AFS Cast Iron Research Committee was 3:1 and 5:1, respectively. A step style casting was selected to accommodate the factor of cooling rate with minimal influence on residual heat flow from a complex geometry casting. The step casting also satisfied the requirement for retooling which, in turn, created an experimental design that maintains a fairly constant surface area but changes the volume based on the design sand to metal ratio.

Using this design intent, solidification models using MagmaSoft™ were generated for the riser design that could satisfy the pouring of ductile and gray iron. Through several riser design iterations, a closed riser design was determined as the optimal design to satisfy feeding requirements for gray and ductile iron castings without adding complexity to the tooling to create molds meeting the sand to metal ratio requirement. Figure 1 shows the final design selected for the investigation of the two sand to metal ratios used in the study. The fabricated mold box used for the project was 24 in. by 19in., 8 ½ in. the cope over a 6 in. drag.

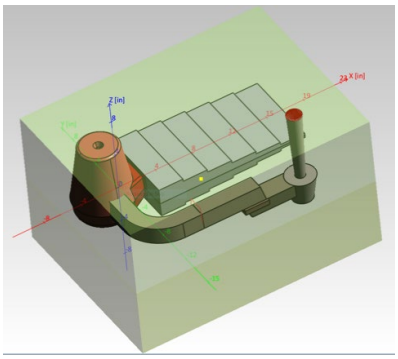

Figure 1. Casting configuration location with respect to the overall 24 in. x 19 in., 8 ½ in. over 6 in. the 1.25% phenolic urethane sand mold. Shown is the 3:1 sand to metal ratio casting. The 5:1 sand to metal ratio casting had the same length, same width, and gating/riser configuration as shown.

AGGREGATE MATERIALS

Three aggregate materials were used in the study. Pure, round grain silica sand was used as the baseline aggregate. Two synthetic aggregates were included in the study. One synthetic aggregate, designated as Aggregate A, is predominantly 70-75% alumina, ~ 10% silica, ~10% black iron oxide, and <5% titanium dioxide content ceramic. The other engineered ceramic aggregate, designated as Aggregate B, is approximately 60-65% alumina, 30-35% silica, ~1% black iron oxide, and ~1% titanium dioxide content ceramic. Manufacturer-supplied screen distribution is provided in Table 1.

Table 1. Screen Distribution of Aggregates

Sieve No.	Silica	Aggregate A	Aggregate B
30	-----	-----	-----
40	1	-----	-----
50	28	22	3.5
70	38	38	39.2
100	21	32	48.3
140	8	8	8.4
200	2	-----	0.6
270	1	-----	-----
AFS GFN	60	58	64
Permeability	NA	108	NA

GFN = grain fineness number.
NA = not available information from product datasheet.

HEAT CAPACITY MEASUREMENTS

Small phenolic urethane coated samples were randomly collected after producing a mold during the ductile iron experiments. The extricated sample was lightly grounded prior to placing the sample inside of a 70-microliter alumina crucible and placed inside of the thermogravimetric analyzer/differential scanning calorimetry (TGA/DSC) machine (Mettler Toledo TGA/DSC 1 STARe System). Sample weight varied but a minimum of 75% alumina capacity was maintained. The method for the samples was ramping the heat up from 25ºC (77ºF) to 1400ºC (2552ºF) at 10ºC (18ºF) per minute under 25 milliliters per minute of high purity nitrogen. Representative heat capacity data for each aggregate is presented in Figure 2.

The heat capacity curves in Figure 2 represent the thermal energy associated with bonded samples of 1.25% phenolic urethane and will be different in characteristic features associated with unbonded silica sand as reported in literature by Svidro, Dioszegi, and Svidro.[4] Using baseline silica as reference, Aggregate A shows a similar thermal curve as baseline silica but shifted approximately 10-20% lower for all temperature measurements. Since Aggregate A has a lower heat capacity, its ability to hold heat is reduced and the aggregate material would be expected towards a faster overall cooling rate. Aggregate B shows a lower heat capacity value at temperatures below 600C (1112F) but higher above this temperature up to 1200C (2192F). For the investigation, it would be expected that Aggregate B would be slightly more insulating than baseline silica because heat saturation of the mold would be sufficient to provide these conditions.

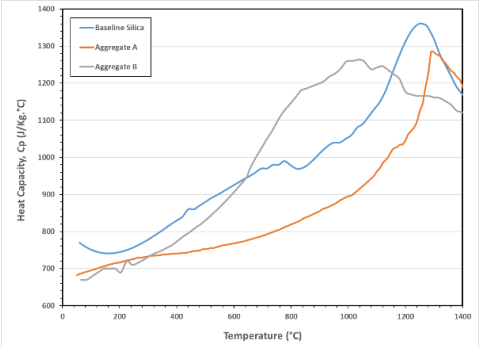

Figure 2. Heat capacity measurements for the three aggregates tested. Phenolic urethane bonded samples were heated using a pure nitrogen atmosphere at a heating rate of 10ºC/min (18ºF/min) heating rate.

MOLD PRODUCTION

The procedure for producing phenolic urethane-based sand molds were identical for all sand to metal ratios investigated and cast iron types. Because of the variety of aggregates used, a 70 lb. vibratory mixer was used to eliminate cross contamination between aggregates if a continuous mixer was used. A target of 1.25% total phenolic urethane content was used for all aggregates with 55% Part 1 to 45% Part 2 ratio. For the baseline silica sand, a 2% liquid amine catalyst based on resin was selected. Because the ceramic aggregates had different pH and acid demand value (ADV) from the silica sand based on the aggregate manufacturer, the liquid amine catalyst was adjusted accordingly. The procedure for mixing the aggregate was identical for aggregate. The dry aggregate was placed in the vibratory mixer and the weighed Part 1

and Part 2 resin based on the sand weight was added to the mixer and mixed for approximately 90 seconds. The resin-coated aggregate was removed and transferred to a holding bucket. This procedure was repeated until the desired total weight of the aggregate for either the cope or drag was prepared. For each bucket, the resin-coated aggregate was placed back in the vibratory mixer and then the catalyst was added. After 15 seconds, the aggregate was removed and immediately transferred to the mold. This procedure was repeated until all the aggregate was prepared. While each bucket of prepared aggregate was added to the mold box, the aggregate was hand packed for uniform densification and continued until the prescribed amount of sand completely filled the cope or drag box. Once completely filled, a strike off bar was used to level the sand.

During the production of the phenolic urethane molds, a thermocouple fixture was secured to the cope frame to accurately locate thermocouples for the metal and tested aggregates. These measurements were only performed for the ductile iron castings. Three type-K thermocouples were placed in the metal. One thermocouple was located at the metal-sand interface, another was located ½" from the interface, and the last thermocouple was located at the mid-point of the section (i.e., the parting line for either the 3:1 or 5:1 sand to metal ratio). Stainless steel rods of similar diameter were used to locate the final position of the thermocouple. The metal designated thermocouples were inserted in the mold during mold assembly, locating the designated position using machinist gauge blocks. Four type-K thermocouples were placed in the sand mold at distances of 1/8", ¼", ½", and 1" from the metal-sand interface. The distances were set prior to making the mold by sliding the designated thermocouple through a compression fitting and then located the appropriate distance with a machinist gauge block. Once the center of the thermocouple bulb was accurately placed, the compression fitting was tightened to prevent movement during the introduction of the resin-coated sand.

METAL PREPARATION

Ductile Iron Production

Base iron was prepared in a 300 lb. induction furnace using primarily Sorel™ pig iron, some low carbon steel punchings to reduce the carbon content to around 3.9%C, and Fe-75%Si to achieve a desired 1.2% Si content in the base iron prior to tapping. Once the base iron temperature reached approximately 2850F (1565C), pure Cu was added to the base iron with a target content of 0.50%. After the copper was added, the pouring ladle was transferred to the Flowtret™ treatment box, and the base iron was poured into the ductile treatment box.

Approximately 5.5 lbs. of Fe-45%Si-3.5%Mg treatment alloy with 2.0 lbs. of Fe-75%Si was used in the treatment reaction chamber. After treatment, the pouring ladle was transferred to the mold, slagged, and poured at 2650F ±10°F (1455C ±6°C). Chemistry for each tested aggregate and sand to metal ratio variable is reported in Table 2.

Table 2. Ductile Iron Chemistry

Heat ID	C	Si	Mn	Cu	P	S	Mg
Silica Sand 3:1 Casting	3.71	2.31	0.06	0.453	0.025	0.014	0.041
Aggregate A 3:1 Casting	3.75	2.32	0.04	0.531	0.024	0.008	0.044
Aggregate B 3:1 Casting	3.69	2.59	0.05	0.549	0.013	0.009	0.043
Silica Sand 5:1 Casting	3.72	2.49	0.03	0.556	0.028	0.007	0.046
Aggregate A 5:1 Casting	3.80	2.43	0.03	0.565	0.017	0.010	0.053
Aggregate B 5:1 Casting	3.79	2.43	0.05	0.533	0.032	0.007	0.058

Gray Iron Production

Similar to the ductile iron production, the gray iron heat was prepared in a 300 lb. induction furnace primarily using gray pig iron of 3.7% C and 2.0% Si. Furnace chemistry was adjusted to the desired iron chemistry by adding low carbon steel punching and Fe-75%Si alloy. Manganese and sulfur were added to the charge prior to melting. Once the base charge was melted and brought to 2650F (1455C), chopped copper wire was added and then tapped into the transferred ladle. The target pouring temperature for all the castings was 2550F ±10°F (1399C ±6°C). Chemistry for each tested aggregate and sand to metal ratio variable is reported in Table 3.

Table 3. Gray Iron Chemistry

Heat ID	C	Si	Mn	Cu	P	S
Silica Sand 3:1 Casting	3.23	2.14	0.337	0.400	0.020	0.067
Aggregate A 3:1 Casting	3.11	1.95	0.359	0.400	0.019	0.063
Aggregate B 3:1 Casting	3.00	2.12	0.415	0.650	0.025	0.098
Silica Sand 5:1 Casting	3.02	2.00	0.430	0.553	0.022	0.076
Aggregate A 5:1 Casting	3.39	2.07	0.494	0.453	0.027	0.071
Aggregate B 5:1 Casting	3.17	2.03	0.464	0.407	0.030	0.055

TENSILE BAR PREPARATION

For both the ductile and gray iron trials, extraction and preparation of ASTM E8 tensile bars were identical. Figure 3 shows the location of the extracted tensile bar for the 3:1 and 5:1 test casting, respectively. Extracted tensile bars were approximately 1 in. (2.54 cm) by 1 in. (2.54 cm) square in cross section and 8 in (20.32 cm) in length. Prior to machining the tensile bars, the square bars were tested for hardness using a Brinell hardness tester on the ends of the bars. The square bars were reduced to ¾ in. (1.9 cm) diameter cylindrical samples as specified by

ASTM E8 on a manual lathe using a four-jaw chuck. A CNC G-Code was written on a Haas L-1 lathe to create the tensile bar profile based on the ASTM E8 specification. Once completed, the tensile bars were transferred to a Satec universal tester to record the strength properties and ductility of tensile bar specimen.

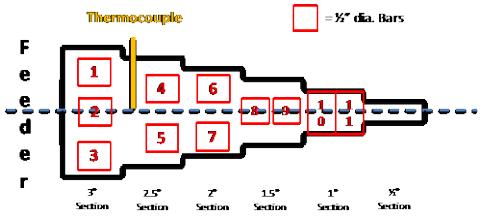

(a) 3:1 Sand to Metal Ratio Test Casting

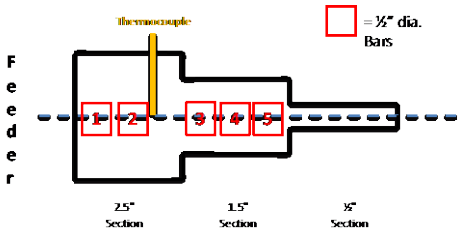

(b) 5:1 Sand to Metal Ratio Test Casting

Figure 3. Location of extracted bars for processing into ASTM E8 tensile bars used to measure the mechanical properties for gray and ductile iron test castings.

PRESENTATION OF DATA

SOLIDIFICATION TIME

The thermocouple location illustrated in Figure 3 was used to determine the solidification time for each experiment. The solidification time was determined by using the numerical first derivative of the recorded temperature and plotting with the temperature profile as shown in Figure 4. All reported solidification profiles were determined using this analysis method. Table 4 provides the estimated solidification time for the ductile experiments. Table 5 gives a partial list of determined solidification times. Times not reported were a result of erroneous thermocouple data or thermocouple failure.

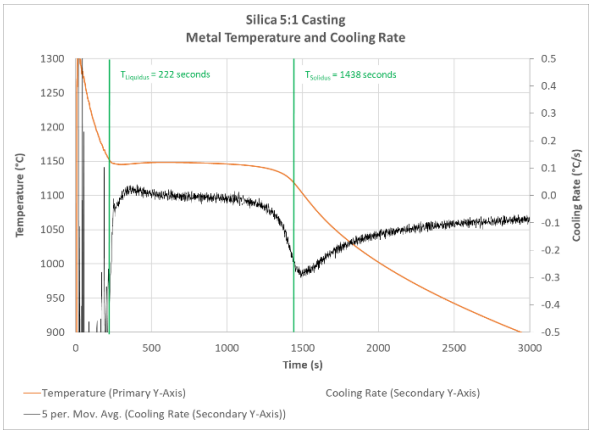

Figure 4. Sample thermal profile and cooling curve analysis were performed to determine the solidification time. The graph was obtained from the ductile iron experiments using the 5:1 casting geometry (thermocouple location shown in Fig. 3(b)) with baseline silica sand.

Table 4. Ductile Iron Solidification Time

Sample ID	*Liquidus Time (s)*	*Solidus Time (s)*	*Solidification Time (s)*
Silica 3:1	271	1893	1622
Ceramic A 3:1	227	1676	1449
Ceramic B 3:1	338	2047	1709
Silica 5:1	222	1438	1216
Ceramic A 5:1	254	1378	1124
Ceramic B 5:1	314	1573	1259

Table 5. Gray Iron Solidification Time

Sample ID	*Liquidus Time (s)*	*Solidus Time (s)*	*Solidification Time (s)*
Silica 3:1	------	-------	------
Ceramic A 3:1	247	1664	1417
Ceramic B 3:1	------	------	------
Silica 5:1	------	------	------
Ceramic A 5:1	133	1163	1030
Ceramic B 5:1	274	1549	1275

METALLURGICAL ANALYSIS

After the tensile bars were fractured using the Satec universal testing machine, a thin section, approximate ½ in. (1.27 cm) in thickness was extracted near the fracture zone. Each bar sample was individually prepared for metallurgical evaluation using the Lecoset™ 100 cold

mount epoxy resin system. The samples were rough ground using an 80-grit belt sander followed by a 180-, 320- and 600-grit polishing wheel. Polishing was accomplished using a 3-micron silk pad polishing wheel followed by a 1-micron red felt polishing wheel. Final buffing was completed using a colloidal silica compound.

After polishing the sample(s), metallurgical analysis was performed on a Zeiss Axiovert 25 microscope equipped with a Paxcam 3 3.1 megapixel camera. Digital analysis was completed using the Leco Pax-It 2, Version 1, analysis software. Gray iron flake analysis used software settings based on the ASTM A247-16a standard. For ductile iron graphite nodule analysis, software settings based on ASTM E2567-16a standard was used. Ferrite determination was completed by first etching the sample with 2% Nital for 10-15 seconds followed by an acetone rinse and hot-air drying. The analysis software determined the ferrite area percent by setting the autodetect settings to recognize white and light gray light. Adjustments were made to the gray setting detection if the highlighted area did not match the image. All photomicrographs and analysis used 100x magnification. A sample of the photomicrograph analysis procedure is presented in Figure 5. As shown in Fig. 5(b), the pearlite microstructure was dark gray and closely related to similar black scale levels of the graphite nodules. The image analysis software was set using the white to light gray region of the photomicrograph to determine %ferrite.

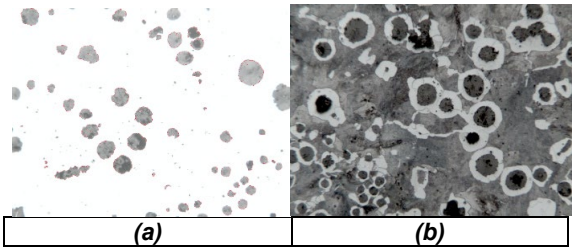

Figure 5. Sample photomicrographs of the technique used to determine the microstructure for data analysis. Photomicrographs shown are from the ductile iron, 5:1 casting, baseline silica sand experiment. (a) Unetched sample used to determine the nodularity and nodule count using ASTM E2567-14A Standard on the image analysis software. (b) Etched sample using 2% Nital etchant to reveal the pearlite microstructure. Both (a) and (b) captured at 100x magnification.

MECHANICAL PROPERTIES

A two-way analysis of variance (ANOVA) model was employed to differentiate the investigated aggregates for the tensile strength, yield strength, and ductility of 80-55-06 ductile iron mechanical properties and tensile strength properties for class 40 gray iron. The two-way ANOVA included material (silica, Aggregate A, and Aggregate B), section (3.0 in. (7.62 cm), 2.5 in (6.35 cm), 2.0 in (5.08 cm), 1.5 in (3.81 cm), vs. 1.0 in. (2.54 cm.), as applicable), and a material and section interaction for the fixed effects for ductile iron. For 3:1 ductile iron casting geometry, a 3 x 5 factorial design was used. For 5:1 ductile iron casting geometry, a 3 x 2 factorial design was used since only 2 sections were included in this case (2.5 in./6.35 cm) vs. 1.5 in./3.81 cm). The statistical package SPSS Statistics®, Version 29.0 was used with a significance level of 0.05 for the analyses. Two-way ANOVA without replication considered only the main factors of section thickness and aggregate material for the class 40 gray iron. The statistical package used for the gray iron analysis was Microsoft Excel® with a significance level of 0.05.

TWO-WAY ANOVA RESULTS FOR 80-55-06 DUCTILE IRON 3 TO 1 SAND TO METAL RATIO EXPERIMENT

Tensile Strength for 3:1 Sand to Metal Ratio Experiment

Figure 6 shows the tensile strength properties obtained from the ductile iron experiment for the 3:1 sand to metal ratio casting. Also, shown in the figure are the measured nodule count and percent ferrite for each section. As expected, the nodule count showed an increasing trend toward the thinner section of 1.5 in. (3.81 cm) and 1.0 in. (2.54 cm.) for all aggregates investigated. Surprisingly, the percent ferrite for all aggregates was higher toward the thinner sections that was expected to induce a higher cooling rate to produce a higher pearlite content. However, this observation was attributed to the casting design where the higher cooling rate induced during solidification before the mold was saturated with heat produces an expected nodule count trend. In the thin sections, carbon diffusion paths between the nodules are shorter and was surmised to deplete the carbon during cooling to the solid-state transformation temperature.

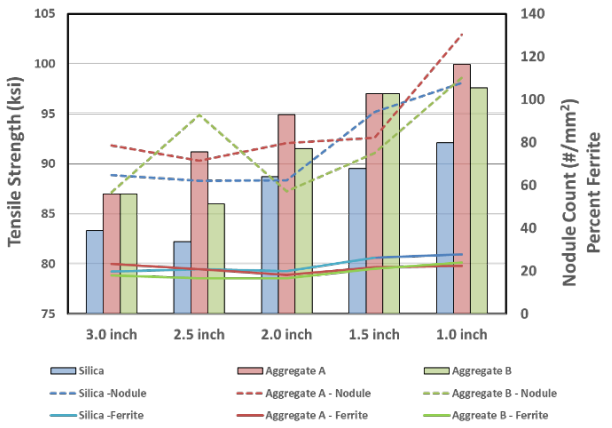

Figure 6. Plot of tensile strength properties, nodule count, and percent ferrite of ductile iron for the 3:1 sand to metal ratio casting as a function of section thickness. Tensile strength, nodule count, and percent ferrite are the averages represented in Fig. 3(a).

From Figure 6, the baseline silica sand exhibited the lowest tensile strength for all section thickness for the 3:1 sand to metal ratio casting. Aggregate A displayed the highest tensile strength for most of the sections.

Aggregate B showed equal or lower tensile strength that Aggregate A. In general, higher nodule count contributed more pronouncedly to the higher tensile strength properties associated with Aggregate A than the ferrite content, especially at the thicker sections of 2.5 in, (6.35 cm) and 3.0 in. (7.62 cm). However, higher pearlite content appears to also contribute to higher tensile strength for the engineered ceramic aggregates tested, particularly at thinner section of 1.0 in (2.54 cm) and 1.5 in. (3.81 cm)

The two-way ANOVA results, generating a R-squared value of 0.921 (adjusted R squared value of 0.859) for tensile strength from the 3:1 ductile iron experiment, indicated there was no significant interaction between material and section on tensile strength ($F(8,18)=1.12$, $p = .395$). However, there was a significant material effect ($F(2,18)=30.53$, $p < .001$), as well as a significant section effect ($F(4,18)=35.50$, $p < .001$). Figure 7 shows the descriptive statistics of tensile strength. For the three pairwise material comparisons, there was a significant difference in tensile strength between Aggregate B and Aggregate A (mean difference = -1.955 psi (-0.013 MPa), p = .040, 95% Confidence Interval (CI): -3.816 psi (-0.026 MPa) to -0.095 (-0.0006 MPa)), a strong significance effect between Silica and Aggregate A (mean difference = -6.564 psi (-0.045 MPa, p < .001, 95% CI: -8.424 psi (-0.058 MPa) to -4.703 psi (-0.032 MPa)), and a similar strong significant effect between Silica and Aggregate B (mean difference = -4.608 (-0.032 MPa), p < .001, 95% CI: -6.469 (-0.045 MPa) to -2.748 (-0.019 MPa)). In terms of differences in tensile strength among the sections, the following results were found. There was no difference between sections 1.0" (2.54 cm) and 1.5" (3.81 cm) ($p = .107$), but each of these smaller sections was significantly different from sections 2.0" (5.08 cm), 2.5" (6.35 cm), and 3.0" (7.62 cm) (p values ranged from <.001 to .032). Section 2.0" (5.08 cm) was significantly different from each of the other sections (p values ranged from <.001 to .032). There was no difference between sections 2.5" (6.35 cm) and 3.0" (7.62 cm) ($p = .533$), but each of these bigger sections was significantly different from sections 1.0" (2.54 cm), 1.5" (3.81 cm), and 2.0" (5.08 cm) (each $p < .001$).

Yield Strength for 3:1 Sand to Metal Ratio Experiment

Figure 8 shows the yield strength properties obtained from the ductile iron experiment for the 3:1 sand to metal ratio casting. Also, shown in the figure are the measured nodule count and percent ferrite for each section.

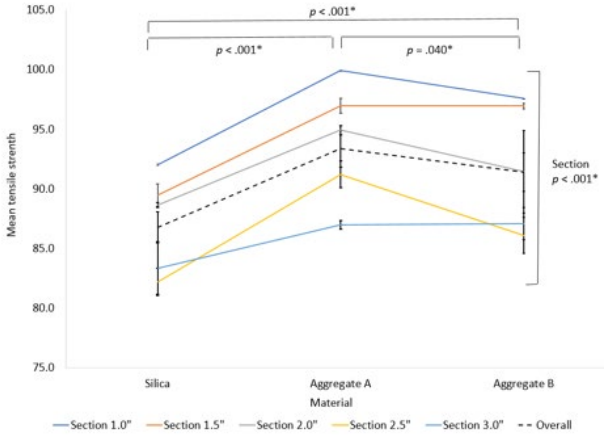

Figure 7. Mean tensile strength (with standard error bars) by section and material for 3:1 ductile iron. Note. The standard errors for each material within section 1.0" were very small (< 0.07) and not showing up in the figure (0.063 for Silica, 0.036 for Aggregate A, and 0.008 for Aggregate B).

Again, for all aggregates investigated, the nodule count showed an increasing trend toward the thinner section of 1.5 in. (3.81 cm) and 1.0 in. (2.54 cm.) that resulted in higher yield strength properties. The engineered ceramic aggregates displayed higher yield strength properties than baseline silica sand. Aggregate B, unlike the trend observed for tensile strength in figure, showed higher yield strength than Aggregate A in the thicker sections of 2.5 in, (6.35 cm) and 3.0 in. (7.62 cm). Aside from the nodule count for the 2.5 in. (6.35 cm) section, the lower ferrite percentage of aggregate may contribute to the higher yield strength properties in thicker sections. For the thinner sections of 2.0 in (5.08 cm) and less, both

ceramic aggregates had comparable yield strength but 5-10% higher than baseline silica sand.

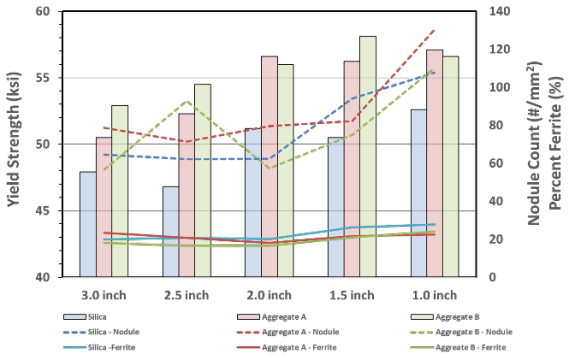

Figure 8. Plot of yield strength properties, nodule count, and percent ferrite of ductile iron for the 3:1 sand to metal ratio casting as a function of section thickness. Shown yield strength, nodule count, and percent ferrite are the averages represented in figure 3(a).

Two-way ANOVA results, producing an R-squared value of 0.923 (adjusted R squared value of 0.864) for tensile strength from the 3:1 ductile iron experiment, showed no interaction effect between material and section on yield strength ($F(8,18)=1.42$, $p = .253$). Significant material effect ($F(2,18)=59.62$, $p < .001$) was statistically observed, as well as a significant section effect ($F(4,18)=21.94$, $p < .001$). Descriptive statistics of yield strength for 3:1 ductile iron by section and material are shown in Figure 9. The mean differences in yield strength for the three pairwise material comparisons displayed a mild significant difference in yield strength between Aggregate B and Aggregate A (mean difference = 1.230 (0.008 MPa), $p = .041$, 95% CI: 0.059 (0.0004 MPa) to 2.402 (0.017 MPa)), strong significance between baseline silica sand and Aggregate A (mean difference = -4.507 (-0.031 MPa), $p < .001$, 95% CI: -5.679 (-0.039 MPa) to -3.336 (-0.023 MPa)), and similar strong significance between baseline silica sand and Aggregate B (mean difference = -5.738 (-0.040 MPa), $p < .001$, 95% CI: -6.909 (-0.048 MPa) to -4.566 (-0.031 MPa)). In terms of differences in yield strength among the sections, there was no significance among sections 1.0” (2.54 cm), 1.5” (3.80 cm), and 2.0” (5.08 cm) (p values ranged from .207 to .561), but each of these smaller sections were significantly different from sections 2.5” (6.35 cm) and 3.0” (7.62 cm) (each p value <.001). No difference between sections 2.5” (6.35 cm) and 3.0” (7.62 cm) ($p = .295$) were observed, but each of these bigger sections were significantly different from sections 1.0” (2.54 cm), 1.5” (3.80 cm), and 2.0” (5.08 cm) (each p value < .001).

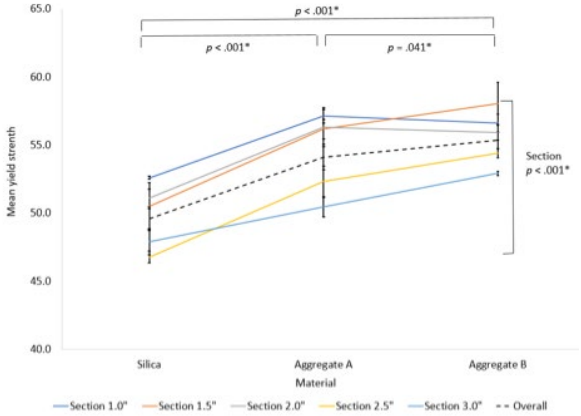

Figure 9. Mean yield strength (with standard error bars) by section and material for 3:1 ductile iron.

Ductility for 3:1 Sand to Metal Ratio Experiment

Figure 10 shows the yield strength properties, in addition to percent ferrite, obtained from the ductile iron experiment for the 3:1 sand to metal ratio casting. For all aggregates tested, the ductility properties increased as the section size decreased. In general, the increase in the observed increase in ductility was inferred to be associated with the increase in the percent ferrite content. As presented in the strength analysis, the nodule count also increased toward a decrease in section thickness, though, increase in nodule count is more associated with improved strength properties than ductility. Baseline silica sand showed higher ductility for all section thickness when compared to the engineered ceramic aggregates. When comparing the ductility properties between the ceramic aggregates, variability between the aggregates was observed. Section 2.5 in (6.35 cm) and 2.0 in (5.08 cm) showed around a 20% higher ductility for Aggregate A compared to Aggregate B, though the 1.0 in (2.54 cm) showed the opposite difference with Aggregate B exhibiting higher ductility. For the remaining sections, Aggregate A and B displayed comparable ductility.

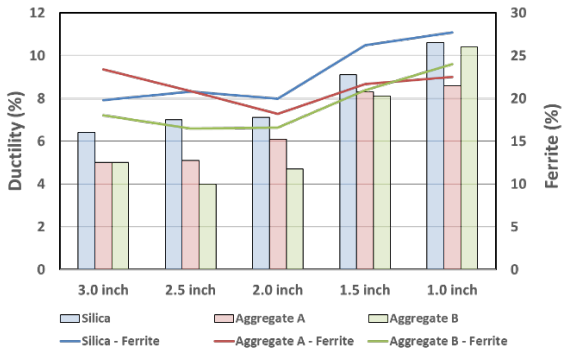

Figure 10. Plot of ductility properties and percent ferrite of ductile iron for the 3:1 sand to metal ratio casting as a function of section thickness. Shown ductility and percent ferrite are the averages represented in Fig. 3(a).

Two-way ANOVA results for ductility from the 3:1 ductile iron experiment produced an R Squared = .889 (Adjusted R Squared = .804). There was a significant material effect ($F(2,18)=9.87$, $p = .001$), as well as a significant section effect ($F(4,18)=29.46$, $p < .001$) on ductility properties from the experiment. However, no significant interaction between material and section on ductility ($F(8,18)=0.90$, $p = .540$) was observed. Descriptive statistics of ductility for 3-1 ductile iron by section and material are shown in Figure 11. For the three pairwise aggregate comparison, there was a significant difference in ductility between Aggregate B and Aggregate A (mean difference = -1.576 %, $p = .001$, 95% CI: -2.442% to -0.709%) and between Silica and Aggregate B (mean difference = 1.607%, $p = .001$, 95% CI: 0.741% to 2.473%). Unlike the analysis for yield and tensile strength, there is no significant difference between Silica and Aggregate A ($p = .939$). In terms of differences in ductility among the sections, section 1.0 in. (2.54 cm) was significantly different from all the other sections (p value ranged from <.001 to .014). Section 1.5 in. (3.81 cm) was significantly different from all the other sections (p value ranged from <.001 to .014). There was no difference between sections 2.0 in (5.08 cm), 2.5 in. (6.35 cm), and 3.0 in. (7.62 cm) (p value ranged from .481 to .894), but each of these bigger sections were significantly different from sections 1.0 in. (2.54 cm) and 1.5 in. (3.81 cm) (each p value < .001).

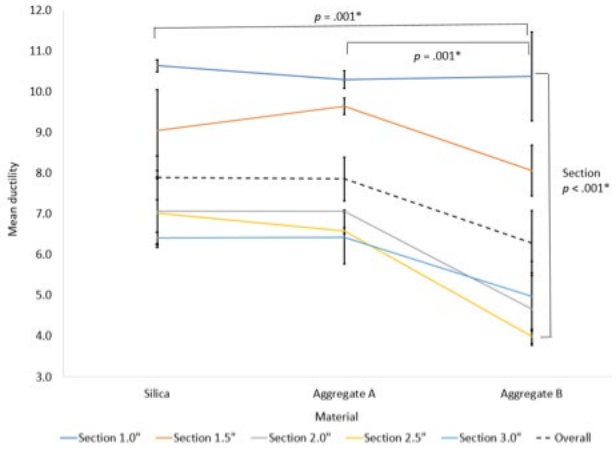

Figure 11. Mean ductility (with standard error bars) by section and material for 3:1 ductile iron.

TWO-WAY ANOVA RESULTS FOR 80-55-06 DUCTILE IRON 5 TO 1 SAND TO METAL RATIO EXPERIMENT

Discussion of the 5-1 sand to metal ratio will be based on the tensile bar location indicated in Figure 3(b). For the general discussion of properties, bar location will be used as the independent variable on the presented graphs to illuminate the mechanical properties variations better. Statistical analysis discussion used the averages of the bar location for the specific casting section thickness to generate data based on the factors of aggregate material and section thickness.

Ductile Iron Tensile Strength for 5:1 Sand to Metal Ratio Experiment

Tensile properties for the 5:1 sand to metal ratio casting for ductile iron is presented in Figure 12. For all section locations, the engineered ceramic aggregates exhibited higher tensile properties than baseline silica sand. Surprisingly, Aggregate B showed the highest tensile properties for all section locations than Aggregate A, opposite to observations analyzed for the 3:1 sand to metal ratio. It is unclear why Aggregate B exhibited higher tensile strength because the solidification time as provided in Table 3 and heat capacity data presented in Figure 2 does not substantiate the observation of higher strength when Aggregate B showed lowest nodule count and highest percent ferrite.

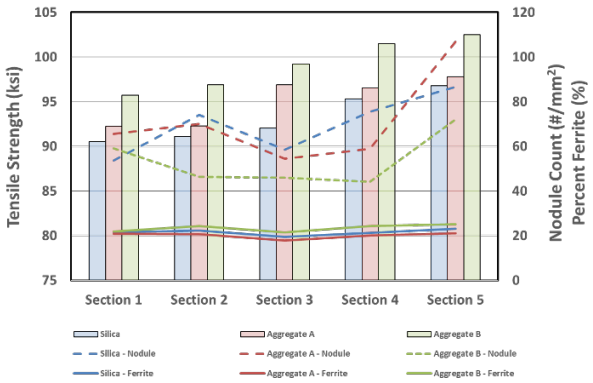

Figure 12. Plot of tensile strength properties, nodule count, and percent ferrite of ductile iron for the 5:1 sand to metal ratio casting as a function of section thickness. Shown tensile strength, nodule count, and percent ferrite are bar location represented in Fig. 3(b).

The two-way ANOVA results for tensile strength from the 5:1 ductile iron experiment with a R Squared = .895 (Adjusted R Squared = .837) showed no significant interaction between material and section on tensile strength ($F(2,9)=0.15$, $p = .866$). Main factor analysis showed a significant aggregate effect ($F(2,9)=20.24$, $p < .001$), as well as a significant section effect ($F(1,9)=33.43$, $p < .001$). Descriptive statistics of tensile strength for 5:1 ductile iron by section and material are shown in Figure 12. Performing a three pairwise material comparisons on the mean differences in tensile strength indicated there was a significant difference in tensile strength between Aggregate B and Aggregate A (mean difference = 4.020 psi (0.027 MPa), $p = .002$, 95% CI: 1.910 psi (0.013 MPa) to 6.130 (0.042 MPa)) and between Silica and Aggregate B (mean difference = -6.020 psi (-0.042 MPa), $p < .001$, 95% CI: -8.130 (-0.056 MPa) to -3.910 (-0.027 MPa)), but not between Silica and Aggregate A ($p = .061$).

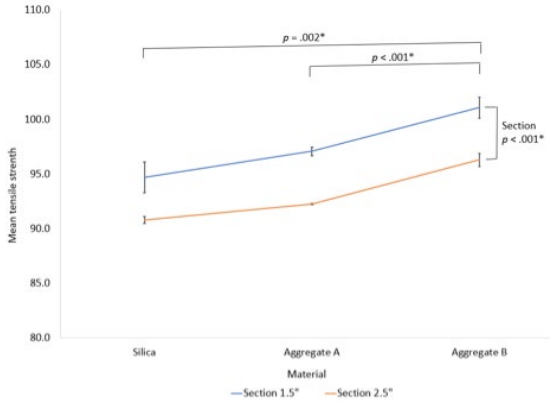

Figure 12. Mean tensile strength (with standard error bars) by section and material for 5:1 ductile iron.

Ductile Iron Yield Strength for 5:1 Sand to Metal Ratio Experiment

Yield strength properties for the 5:1 sand to metal ratio casting for ductile iron is presented in Figure 13. For the 1.5 in (3.80 cm) section location (section 3 through 5), both engineered ceramic aggregates exhibited higher yield strength properties than baseline silica sand except for section 3 for Aggregate A that showed a comparable yield strength to the baseline silica sand. Aggregate A exhibited comparable yield strength for the 2.5 in. (6.35 cm) section (section 1 and 2) and Aggregate B showed a 5-8% increase of yield strength when compared to baseline silica sand.

When comparing the 1.5 in (3.80 cm) and 2.5 in. (6.35 cm) section in Figure 12 for the analysis of the tensile properties in section titled Tensile Strength for 5:1 Ductile Iron Experiment, both sand to metal exhibited a similar 5-8% increase in yield strength between Aggregate A and B. However, comparable to slightly higher yield strength properties were observed in the 5:1 sand to metal ratio between Aggregate A and baseline silica. For the similar thickness for the 3:1 sand to metal ratio, Aggregate A showed between a 10-15% increase in yield strength properties. A noticeable difference in yield strength properties for the 3:1 sand to metal ratio was observed but was not largely apparent in the 5:1 sand to metal ratio for Aggregate A and baseline silica sand. Unfortunately, the nodule count and percent ferrite data does not fully support why the yield strength properties are noticeably higher than Aggregate A and baseline silica sand.

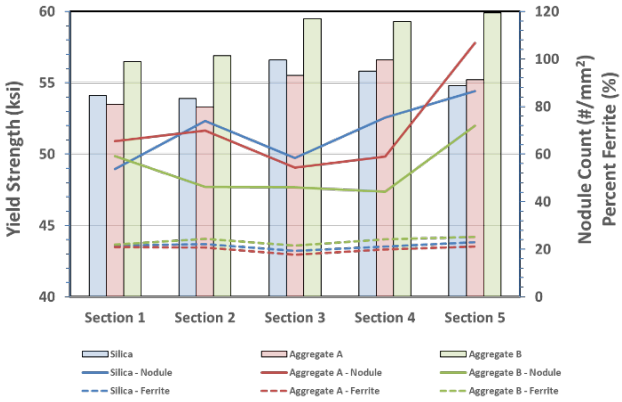

Figure 13. Plot of yield strength properties, nodule count, and percent ferrite of ductile iron for the 5:1 sand to metal ratio casting as a function of section thickness. Shown tensile strength, nodule count, and percent ferrite are bar locations in Fig. 3(b).

Two-way ANOVA results for yield strength from the 5:1 ductile iron experiment with a R Squared = .953 (Adjusted R Squared = .927). First, there was not a significant interaction between aggregate and section on tensile strength ($F(2,9)=1.15$, $p = .358$). However, there was a significant aggregate effect ($F(2,9)=55.68$, $p < .001$), as well as a significant section effect ($F(1,9)=57.86$, $p < .001$). Descriptive statistics of yield strength for 5:1 ductile iron by section and material are shown in Figure 14.

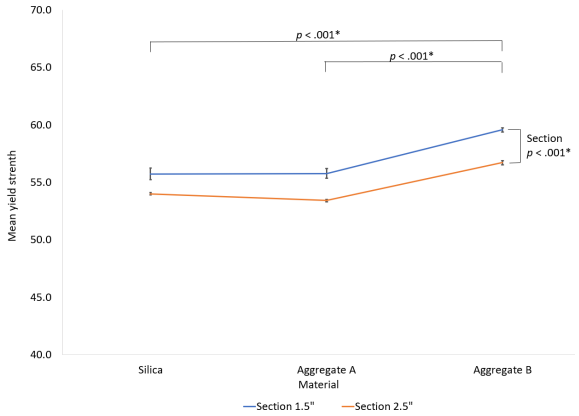

Figure 14. Mean yield strength (with standard error bars) by section and material for 5:1 ductile iron.

Three pairwise aggregate comparisons analysis showed there was a significant difference in yield strength between Aggregate B and Aggregate A (mean difference = 3.600, $p < .001$, 95% CI: 2.771 to 4.429) and between Silica and Aggregate B (mean difference = -3.380, $p < .001$, 95% CI: -4.209 to -2.551), but not between Silica and Aggregate A ($p = .563$). In terms of differences in yield strength among the two sections, there was a significant difference in yield strength between the two sections 1.50” (3.80 cm) and 2.50” (6.35 cm).

Ductile Iron Ductility for 5:1 Sand to Metal Ratio Experiment

Yield strength properties for the 5:1 sand to metal ratio casting for ductile iron is presented in Figure 15. Aggregate B generally showed a 10-25% higher elongation properties than silica sand except for section 1, section closest to the feeder. This exception was also true for Aggregate A and all aggregates exhibited comparable ductility in section 1. Aggregate A showed slightly higher ductility in section 2 and 3 but comparable ductility in section 4 and 5 when compared to baseline silica sand. A lower nodule count and slightly higher percent ferrite may be attributable to the comparable or higher ductility properties observed for the engineered ceramic aggregates.

Figure 15. Plot of ductility properties, nodule count, and percent ferrite of ductile iron for the 5:1 sand to metal ratio casting as a function of section thickness. Shown tensile strength, nodule count, and percent ferrite are bar location represented in Figure 3(b).

Two-way ANOVA results for ductility from the 5:1 ductile iron experiment with a R Squared = .421 (Adjusted R Squared = .099). There was not a significant interaction between aggregate and section on ductility ($F(2,9)=0.53$ $p = .608$). Additionally, there was no significant aggregate effect ($F(2,9)=1.18$, $p = .351$) nor a significant section effect ($F(1,9)=2.34$, $p = .160$) was determined. Descriptive statistics of ductility for 5:1 ductile iron by section and material are shown in Figure 16. Three pairwise aggregate comparison analysis was not performed because of no statistical analysis with main factor and interactions were determined.

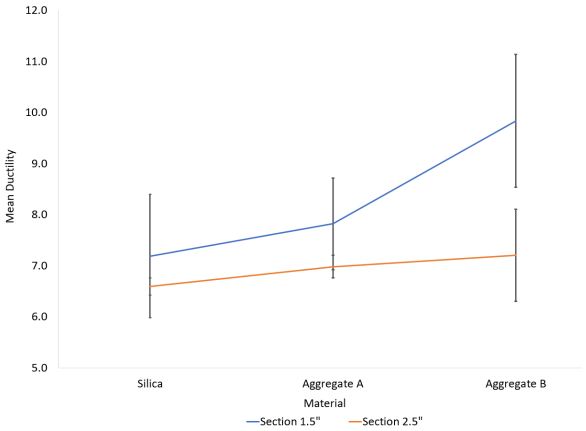

Figure 16. Mean ductility (with standard error bars) by section and material for 5:1 ductile iron.

TWO-WAY ANOVA RESULTS FOR CLASS 40 GRAY IRON EXPERIMENTS

For the gray iron mechanical properties evaluation, an ANOVA statistical analysis was performed but, because of some gaps in the data collection, pairwise aggregate comparison analysis was not performed.

Gray Iron Tensile Strength for 3-1 Sand to Metal Ratio Experiment

Figure 17 shows the average tensile strength properties obtained from the gray iron experiment for the 3:1 sand to metal ratio casting. Also, shown in the figure is the average percent ferrite for each section. In general, baseline silica sand exhibited higher tensile properties than the engineered ceramic aggregates. Thicker sections of 2.5 in and 3.0 in exhibited silica sand having the highest tensile strength, Aggregate A had a 3-5% decrease in strength when compared to silica, and Aggregate B had a 5-7% decrease in strength when compared to silica sand.

For the middle section of the casting at 2.0 in section thickness, silica sand tensile properties were comparable to Aggregate B and Aggregate A had a 2-3% improvement in strength properties. Though gaps existed in the strength data for the thinner section of 1.5 in and 1.0 in section, the ceramic aggregates showed a general trend of 2-6% reduction in tensile strength properties when compared to silica sand. It is unclear why baseline silica exhibited based on the percent ferrite for each section.

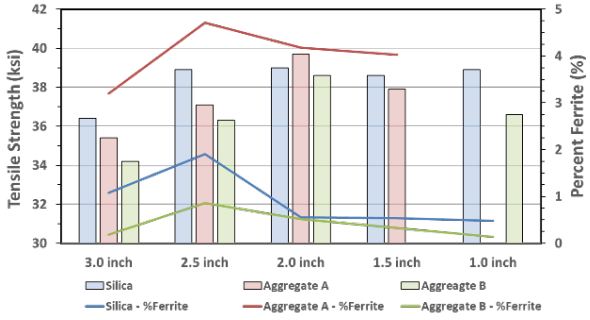

Figure 17. Plot of tensile strength properties and percent ferrite of gray iron for the 3:1 sand to metal ratio casting as a function of section thickness. The shown tensile strength and percent ferrite are the averages represented in figure 3(a).

Statistical analysis using ANOVA Two-Factor without replication indicated a general trend of main factor significance for aggregate and section thickness. Main factor analysis between baseline silica sand and Aggregate A showed no significant aggregate effect ($F(1,3)=1.80$, $p = 0.27$), but a possibly mild significant section effect ($F(3,3)=7.65$, $p = .06$). For the main factor analysis between baseline silica sand and Aggregate B, main factor effect for aggregate showed significance ($F(1,3)=14.12$, $p = 0.03$), and significant effect for section thickness ($F(3,3)=8.74$, $p = .05$). Statistical analysis between Aggregate A and Aggregate B indicated aggregate significance ($F(1,3)=73.92$, $p = 0.01$), and significant effect for section thickness ($F(3,3)=439$, $p = .01$).

Gray Iron Tensile Strength for 5-1 Sand to Metal Ratio Experiment

Figure 18 shows the average tensile strength properties obtained from the gray iron experiment for the 3:1 sand to metal ratio casting. Also, shown in the figure is the average percent ferrite for each section. Dissimilar to the observations noted for the 3-1 sand to metal ratio experiment, the engineered ceramic sand Aggregate B exhibited a 3-13% increase in tensile strength compared to baseline silica sand. The lower percent strength improvement was closer to the feeder and higher strength increased farther away from the feeder toward the thinner section of the casting.

For Aggregate A, a 10-18% improvement in tensile strength was observed when compared to baseline silica sand. As noted for Aggregate B, higher tensile strength properties were more prevailing toward the thinner sections opposite of the feeder for Aggregate A. When comparing Aggregate A to Aggregate B, Aggregate A showed a 2-7% higher tensile strength properties than Aggregate B. From Figure 18, the higher strength properties of Aggregate A could contribute to higher pearlite content. However, the percentage ferrite content of aggregate compared to silica sand does not corroborate the higher tensile strength properties.

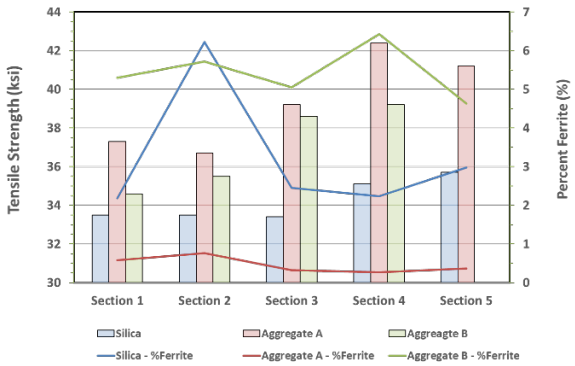

Figure 18. Plot of tensile strength properties and percent ferrite of gray iron for the 5:1 sand to metal ratio casting as a function of section thickness. Shown tensile strength and percent ferrite are bar location represented in Figure 3(b).

Statistical analysis using ANOVA Two-Factor without replication indicated a general trend of main factor significance for aggregate and section thickness. Main factor analysis between baseline silica sand and Aggregate A showed strong significant aggregate effect ($F(1,3)=48.60$, $p = 0.002$), and no section effect ($F(3,3)=4.31$, $p = .09$). For the main factor analysis between baseline silica sand and Aggregate B, the main factor effect for aggregate showed mild significance ($F(1,3)=10.86$, $p = 0.05$), and no significant effect for section thickness ($F(3,3)=2.28$, $p = .26$). Statistical

analysis between Aggregate A and Aggregate B indicated mild aggregate significance ($F(1,3)=9.87$, $p = 0.05$), and significant effect for section thickness ($F(3,3)=14.60$, $p = .03$).

DISCUSSION OF RESULTS

Statistical analysis and general observations indicate engineered ceramic aggregates do have an influence on mechanical properties for gray and ductile iron. Ductile iron castings showed higher strength properties and lower ductility for the ceramic aggregates than the baseline silica sand. However, for gray iron castings, tensile strength properties were observed to be opposite for the 3:1 sand to metal ratio, where baseline silica sand were slightly higher than the ceramic aggregates. For the 5:1 gray iron casting, tensile strength properties in ceramic aggregate molds were 10-20% higher than silica sand.

Unfortunately, the solidification time presented in Table 3 for the ductile iron castings does not fully corroborate the statistical analysis of properties and data observations. Using baseline silica sand as a reference point, the lower solidification time of Aggregate A would support the higher strength properties and lower ductility presented in the data analysis section. However, Aggregate B showed the highest solidification time and does not support higher observed strength properties and lower ductility based on a solidification analysis approach. Difficulty arises further in analyzing Aggregate B performance based on the solid state transformation reaction of ferrite and pearlite. Some of the data does show a higher pearlite content in Aggregate B, particularly with the 3:1 sand to metal ratio, but the 5:1 sand to metal ratio, as with the solidification time, does not have sound evidence on the solid transformation mechanical properties contribution.

For the ductile iron castings investigated, the engineered ceramic aggregates on properties of tensile and yield strength performed 5-10% higher than silica sand for both sand to metal ratio castings. Strength properties for Aggregate A for the 3:1 sand to metal ratio were higher than Aggregate B while ductility was comparable between both ceramic aggregates. When the sand to metal ratio changed to 5:1 casting geometry, the ceramic aggregates performed better than the baseline silica sand, but the strength properties were higher for Aggregate B than Aggregate A. Ductility was comparable or slightly higher for Aggregate B than Aggregate A.

Gray iron castings appear to show sensitivity with respect to sand to metal ratio. For the 3:1 sand to metal ratio, baseline silica sand showed a 2-7% higher tensile strength than the engineered ceramic aggregate except for the tensile bar specimens extracted from the 2.0” (5.08 cm). It also appears for this sand to metal ratio that tensile properties near the feeder of baseline silica sand exhibited a 3-7% higher strength than the ceramic aggregates, but strength properties were only 2-4% higher in the 1.5 in (3.80 in) section. Tensile properties for 5:1 sand to metal ratio exhibited 7-17% higher properties than base line silica sand. Aggregate A performed approximately 2-8% higher than Aggregate B depending on bar location, though the center bar strength properties were comparable between the two ceramic aggregates.

CONCLUSIONS

Analysis for gray and ductile iron mechanical properties between baseline silica sand and engineered ceramic sands show statistical significance, though performance between the two ceramic aggregates varied. Higher strength properties and lower ductility were observed for ductile iron castings cast in ceramic aggregates when compared to the baseline silica. Additionally, when the sand to metal ratio changed, the ceramic aggregate generally had higher strength properties and lower ductility than the baseline silica sand.

For gray iron castings, results were more variable than the ductile iron castings. For the 3:1 casting geometry used for gray iron, baseline silica sand strength properties were either slightly higher or comparable to the ceramic aggregates. When the geometry changed to 5:1 sand to metal ratio, strength cast in the ceramic aggregates was 7-17% higher than the silica sand. Though not statistically analyzed, the sand to metal ratio appears to have a significant effect on the strength properties of gray iron.

ACKNOWLEDGMENTS

The authors acknowledge the American Foundry Society and Ductile Iron Society for sponsoring the research project. Recognition of their technical guidance and contribution to the data analysis are extended to the AFS project steering committee members. They are Brandon Reneau, Matt Meyer, Lizeth Medina, and Anhua Yu. Companies providing material donations are recognized for their support of the project. They are Caterpillar, Neenah Foundry, John Deere Foundry, Elkem, MAGMA Foundry Technologies, and American Pattern. Undergraduate students benefiting from the training provided in the research activities were Maria Alverio, Susan Alverio, Jared Harms, Matt Kapka, Kyle Schick, Mary (McCoy) Primer, Jennifer Curtis, Thayer Prum, and Huessin Alshabib. Your contributions and efforts toward the research activities were greatly appreciated.

REFERENCES

1. "AFS Research: Moving the Industry Forward," AFS News (March 28, 2018). https://www.afsinc.org/news/2018/03/28/afs-research-moving-industry-forward (Link last accessed 01-07-2025.)
2. Ramrattan, S. and Raval, M., "A Casting Trial to Evaluate Alternative Green Sand Systems for Surface Finish and Erosion Defects," *AFS Proceedings of the 123rd Metalcasting Congress*, Paper 19-122 (2019).
3. Ravi, S. and Thiel, J., "Evaluation of Alternate Aggregates for Use in Green Sand and Core Sand Processes," *AFS Transactions*, vol. 128, Paper 20-058, p. 187-199 (2020).
4. Svidro, J., Dioszegi, A., and Svidro, J.T. "The Origin of Thermal Expansion Differences in Various Size Fractions of Silica Sand," *International Journal of Cast Metals Research*, vol. 33, Issue 6, pp. 242-249 (2020).https://www.tandfonline.com/doi/full/10.1080/13640461.2020.1838078#abstract (Link last accessed 01-07-2025.)